Journal of Radiation and Nuclear Application
An International Journal

http://dx.doi.org/10.18576/jnra/060201

Amplitude Analysis of $\gamma N \to \pi N$ Observables Near Threshold

Tarfa H. Alsheddi

Physics Department, College of Science, King Faisal University, Al-Ahsa 31982, P.O. Box 400, Saudi Arabia

Received: 22 Jan. 2021, Revised: 13 April 2021, Accepted: 19 April 2021
Published online: 1 May 2021

Abstract: Amplitude analysis of unpolarized differential cross section and polarization observables for the pion photoproduction reaction on the nucleon near threshold are studied. We investigate whether the uncertainties caused by the use of different $\gamma N \to \pi N$ amplitudes for the predictions of polarization observables in the $\gamma d \to \pi NN$ and $\gamma d \to \pi^0 d$ reactions are also seen in the analysis of observables for pion photoproduction on the nucleon. For this purpose, three different realistic models for the $\gamma N \to \pi N$ amplitude are considered. These models are the unitary dynamical Dubna-Mainz-Taipei DMT-2001 model, the unitary isobar MAID-2007 model, and the chiral MAID (χMAID-2013) model. It has been found that the $\gamma N \to \pi N$ observables are sensitive to the production amplitude, specially at photon energies close to pion threshold.

Keywords: Meson production, Photoproduction reactions, Polarization phenomena in reactions, Spin observables, Polarized beams, Polarized targets.

1 Introduction

The study of pion photo- and electroproduction reactions is of great interest in the field of intermediate-energy nuclear physics. Studying these processes is one facet of the physicists' quest to understand the fundamental strong force which plays the prominent role in interactions between elementary particles at very small distance scales. This study assists in understanding several issues regarding this grand path of comprehending theory for the strong interactions – Quantum Chromodynamics (QCD). One of these is the structure and nature of the QCD bound states. There are two kinds of bound states in QCD: mesons (like the pion or the kaon) and hadrons, which includes nucleons (protons or neutrons) and nucleon resonances (excited states of nucleons) such as the delta particle. The processes of meson photoproduction are excellent tools in studying these states since these reactions proceed through the exchange of QCD bound states. For example, the pion photoproduction in a certain energy regime occurs as a result of the exchange of a delta resonance. By studying this process, we can have insights into the nature of this resonance and the mechanisms by which it interacts and decays [1,2].

An investigation of photoproduction of pions on nucleons yields information on the strong interaction between the nucleons and the mesons, and on the electromagnetic properties of the elementary particles. Pion photoproduction from a single nucleon can be a powerful tool for the study of the structure of the low-energy baryon spectrum in terms of quarks and gluons. In view of the basic importance of the pion for our understanding of nucleons and nuclear forces, pion photoproduction has been and will be of considerable interest. Since this reaction is sensitive to the off-shell properties of the pion-nucleon interactions, i.e. to the short-range behavior of the pion wave function, it may serve as a critical test of models of hadrons [2].

The electromagnetic production of pions on the nucleon, including photoproduction and electroproduction, has long been studied since the publication of the pioneering work of Chew, Goldberger, Low and Nambu (CGLN) [3]. Recently, theoretical interest in these reactions was revived by the new generation of high-intensity and high duty-cycle electron accelerators. With the developments of these new facilities, it is now possible to obtain accurate data for meson electromagnetic production, including spin-dependent observables. Extensive work during these

* Corresponding author e-mail: talsheddi@kfu.edu.sa

more than sixty years [1,4,5,6,7,8,9,10,11,12,13,14,15,16,17,18,19,20,21,22,23,24,25,26,27,28,29,30,31] indicates that, below 500 MeV incident photon energy, the dominant mechanisms of the $\gamma N \to \pi N$ reaction are the Born terms and the $\Delta(1232)$ excitation. Kroll and Rudermann [32] were the first to derive model-independent predictions in the threshold region, so-called low-energy theorems (LET), by applying gauge and Lorenz invariance to the reaction $\gamma N \to \pi N$. The general formalism for this process was developed by Chew *et al.* [3] (CGLN-amplitudes). Fubini *et al.* [33] extended the earlier predictions of LET by including also the hypothesis of a partially conserved axial current (PCAC). In this way they succeeded in describing the threshold amplitude as a power series in the ratio $m = m_\pi/M_N$ up to terms of order m^2. Berends *et al.* [4] analyzed the existing data in terms of a multipole decomposition and presented tables of the various multipole amplitudes constructing in the region up to excitation energies of 500 MeV.

It was found in Ref. [34] that considerable dependences of the $\gamma d \to \pi NN$ observables near π-threshold on the $\gamma N \to \pi N$ amplitude have been obtained. Most recently, Darwish *et al.* [35] found also that the $\gamma d \to \pi^0 d$ observables near π-threshold are also sensitive to the choice of $\gamma N \to \pi N$ amplitude. Therefore, the main goal of the present work is to investigate whether the uncertainties caused by the use of different $\gamma N \to \pi N$ amplitudes for the predictions of $\gamma d \to \pi NN$ and $\gamma d \to \pi^0 d$ observables are also seen in the analysis of pion photoproduction on the free nucleon $\gamma N \to \pi N$. For this purpose, we use three different realistic models for the $\gamma N \to \pi N$ amplitude. These models are the unitary dynamical Dubna-Mainz-Taipei (DMT-2001) [28], the unitary isobar MAID-2007 introduced in Ref. [29], and the chiral MAID (χMAID-2013) [30].

The structure of this paper is organized as follows. In section 2, we briefly outline the formalism used to describe the $\gamma N \to \pi N$ reaction. Section 3 is devoted to the main results for the unpolarized differential cross section $d\sigma/d\Omega_\pi$, the linear photon Σ-asymmetry, the the helicity E-asymmetry, and the double polarization F-asymmetry for the reaction channels $\gamma n \to \pi^0 n$, $\gamma p \to \pi^0 p$, $\gamma n \to \pi^- p$, and $\gamma p \to \pi^+ n$ in the photon energy region near threshold. Finally, we summarize our results in section 4.

2 Formalism

In this section, we describe the theoretical formulation used in our investigation of pion photoproduction on the nucleon, $\gamma N \to \pi N$. The general form of the two-body reaction is

$$a(p_a) + b(p_b) \to c(p_c) + d(p_d)\,, \tag{1}$$

where $p_i = (E_i, \vec{p}_i)$ denotes the four-momentum of particle "i" with $i \in \{a,b,c,d\}$. The total four-momentum is conserved in this reaction and gives $p_a + p_b = p_c + p_d$. Particles a and b can be a photon and a nucleon in the case of pion photoproduction on the nucleon. Particles c and d can be a pion and a nucleon in this case.

In order to compare the theoretical predictions with experimental data one has to evaluate the corresponding cross section. Following the conventions of Bjorken and Drell [36] the general form for the differential cross section of a two-particle reaction in the center-of-mass (c.m.) system is given by [2]

$$\frac{d\sigma}{d\Omega_c} = \frac{1}{(2\pi W)^2}\,\frac{p_c F}{p_a s} \sum_{\mu_d \mu_c \mu_b \mu_a} \left| \mathscr{M}^{fi}_{\mu_d \mu_c \mu_b \mu_a}(\vec{p}_d, \vec{p}_c, \vec{p}_b, \vec{p}_a) \right|^2 \tag{2}$$

with $\mathscr{M}^{fi}_{\mu_d \mu_c \mu_b \mu_a}$ the reaction matrix, μ_i denotes the spin projection of particle "i" on some quantization axis, and

$$F = \frac{E_a E_b E_c E_d}{F_a F_b F_c F_d}\,, \tag{3}$$

where F_i is a factor arising from the covariant normalization of the states and its form depends on whether the particle is a boson ($F_i = 2E_i$) or a fermion ($F_i = E_i/m_i$), where E_i and m_i are its energy and mass, respectively. The factor $s = (2s_a+1)(2s_b+1)$ takes into account the averaging over the initial spin states, where s_a and s_b denote the spins of the incoming particles a and b, respectively. Note that $p_{a,c}$ means $|\vec{p}_{a,c}|$. All momenta are functions of the invariant mass of the two-body system W, i.e. $p_i = p_i(W)$.

For the two-body scattering processes, it is more convenient to use non-covariant normalization of the states and to switch to a coupled spin representation replacing the $\mathscr{M}$-matrix by the $\mathscr{T}$-matrix via

$$\mathscr{M}^{fi}_{\mu_d \mu_c \mu_b \mu_a}(\vec{p}_d, \vec{p}_c, \vec{p}_b, \vec{p}_a) = (2\pi)^3 \sqrt{F_a F_b F_c F_d} \times \sum_{S' \mu'_{S'} S \mu_S} C^{s_c s_d S'}_{\mu_c \mu_d \mu'_{S'}} C^{s_a s_b S}_{\mu_a \mu_b \mu_S}\, \mathscr{T}^{fi}_{S' \mu'_{S'} S \mu_S}(\vec{p}_d, \vec{p}_c, \vec{p}_b, \vec{p}_a)\,, \tag{4}$$

with $C^{s_c s_d S'}_{\mu_c \mu_d \mu'_{S'}}$ as appropriate Clebsch-Gordan coefficient. As next step we introduce a partial wave representation of the $\mathscr{T}$-matrix which reads with $\vec{p}\,'$ and $\vec{p}$ as the final and initial relative momenta, respectively,

$$\mathscr{T}^{fi}_{S' \mu'_{S'} S \mu_S}(W, \vec{p}\,', \vec{p}\,) = \sum_{\ell' \ell J} X^{\ell' \ell J}_{S' \mu'_{S'} S \mu_S}(\hat{p}\,', \hat{p})\, T^{\ell' \ell J}_{fi}(W, p', p)\,, \tag{5}$$

where we have introduced

$$X^{\ell' \ell J}_{S' \mu'_{S'} S \mu_S}(\hat{p}\,', \hat{p}) = \sum_{\mu'_{\ell'} \mu_\ell \mu_J} Y_{\ell' \mu'_{\ell'}}(\hat{p}\,')\, Y^*_{\ell \mu_\ell}(\hat{p})\, C^{\ell' S' J}_{\mu'_{\ell'} \mu'_{S'} \mu_J}\, C^{\ell S J}_{\mu_\ell \mu_S \mu_J}\,. \tag{6}$$

Here ℓ and J denote the orbital and total angular momenta of the system, respectively, $Y_{\ell\mu}(\hat{p})$ a spherical harmonics, and $\hat{p} = (\theta_{\vec{p}}, \phi_{\vec{p}})$.

The partial wave $\mathscr{T}$-matrix is obtained as solution of the LS equation [37]

$$\mathscr{T}^{\ell' \ell J}_{fi}(W, p', p) = V^{\ell' \ell J}_{fi}(p', p) + \sum_{n \ell''} 2m_n \int_0^\infty dp''_n\, (p''_n)^2\, \frac{V^{\ell' \ell'' J}_{fn}(p', p''_n)\, T^{\ell'' \ell J}_{ni}(W, p''_n, p)}{q_n^2 - (p''_n)^2 + i\varepsilon}\,, \tag{7}$$

where $V_{fi}^{\ell' \ell J}(p', p)$ is the interaction potential between the particles and "n" labels possible intermediate two-particle configurations with total mass M_n, reduced mass m_n, and with relative c.m. momentum

$$q_n = \sqrt{2m_n (W - M_n)}. \tag{8}$$

Now, we focus on pion photoproduction on the nucleon

$$\gamma(k, \vec{\varepsilon}_\lambda) + N(p_i) \to \pi(q) + N(p_f), \tag{9}$$

where $k = (E_\gamma, \boldsymbol{k})$, $q = (E_\pi, \boldsymbol{q})$, $p_i = (E_i, \boldsymbol{p}_i)$, and $p_f = (E_f, \boldsymbol{p}_f)$ denote the four-momenta of the incident photon, outgoing pion, initial and final nucleons, respectively. The circular polarization vector of the incoming photon is defined by $\vec{\varepsilon}_\lambda$ with $\lambda = \pm 1$. The F_i factor is given by

$$F_a = 2E_\gamma, \quad F_b = E_i/M_N, \quad F_c = 2E_\pi, \quad F_d = E_f/M_N \tag{10}$$

denoting the nucleon mass by M_N. Therefore, one finds $s = 4$ taking into account the averaging of the cross section over the initial two possible polarizations of the real photon and the two spin projections of the nucleon. Then, the differential cross section is given by

$$\frac{d\sigma}{d\Omega_\pi} = \left(\frac{M_N}{4\pi W}\right)^2 \frac{q}{k} \frac{1}{4} \sum_{\mu_f' \mu_i \lambda} \left| \mathscr{M}^{fi}_{\mu_f' \mu_i \lambda}(\boldsymbol{p}_f, \boldsymbol{q}, \boldsymbol{p}_i, \boldsymbol{k}) \right|^2 \tag{11}$$

The amplitude for pion photoproduction on the nucleon is determined by the current and can be written as a sum of four independent invariant amplitudes as follows [38]

$$\begin{aligned} M^{fi} &= \varepsilon \cdot j(k, p_f, p_i, q) \\ &= \bar{u}_f(p_f) \sum_{j=1}^{4} \mathscr{A}_j(s,t)\, \mathscr{M}_j\, u_i(p_i), \end{aligned} \tag{12}$$

where the covariant operators $\mathscr{M}_j$ are defined by

$$\mathscr{M}_1 = \frac{1}{2} \gamma_5 [k \cdot \gamma, \gamma \cdot \varepsilon] \tag{13}$$

$$\mathscr{M}_2 = \gamma_5 (p_f \cdot \varepsilon - \frac{k \cdot p_f}{k \cdot k} k \cdot \varepsilon) \tag{14}$$

$$\mathscr{M}_3 = \gamma_5 (\gamma \cdot \varepsilon\, k \cdot p_f - k \cdot \gamma\, p_f \cdot \varepsilon) \tag{15}$$

$$\mathscr{M}_4 = \gamma_5 (\gamma \cdot \varepsilon\, k \cdot p_i - k \cdot \gamma\, p_i \cdot \varepsilon). \tag{16}$$

Here, the nucleon spinors are defined by

$$u_i(p_i) = N_i \begin{pmatrix} 1 \\ \frac{\boldsymbol{\sigma} \cdot \boldsymbol{p}_i}{E_i + M_N} \end{pmatrix} \chi_i \tag{17}$$

and

$$u_f(p_f) = N_f \begin{pmatrix} 1 \\ \frac{\boldsymbol{\sigma} \cdot \boldsymbol{p}_f}{E_f + M_N} \end{pmatrix} \chi_f \tag{18}$$

in covariant normalization, with initial and final nucleon momenta $p_{i/f} = (E_{i/f}, \boldsymbol{p}_{i/f})$, corresponding normalization factors $N_{i/f}^2 = (E_{i/f} + M_N)/2M_N$, respectively, denoting the Pauli spin spinors by $\chi_{i/f}$. Four-vector scalar products are denoted by $x \cdot y = x_0 y_0 - \boldsymbol{x} \cdot \boldsymbol{y}$, and three-vectors by boldface characters.

In terms of the CGLN amplitudes F_i [3] the current reads

$$\begin{aligned} \boldsymbol{j}(k, p_f, p_i, q) = \frac{4\pi W}{M_N} \chi_f^\dagger \Big(& i \boldsymbol{\sigma}_T F_1 + (\boldsymbol{\sigma} \cdot \hat{\boldsymbol{q}})(\boldsymbol{\sigma} \times \hat{\boldsymbol{k}}) F_2 \\ & + i \boldsymbol{q}_T (\boldsymbol{\sigma} \cdot \hat{\boldsymbol{k}}) F_3 + i \boldsymbol{q}_T (\boldsymbol{\sigma} \cdot \hat{\boldsymbol{q}}) F_4 \Big) \chi_i, \end{aligned} \tag{19}$$

where $\hat{\boldsymbol{a}} = \boldsymbol{a}/|\boldsymbol{a}|$ denotes a unit vector along $\boldsymbol{a}$, and $\boldsymbol{a}_T = \boldsymbol{a} - (\boldsymbol{a} \cdot \hat{\boldsymbol{k}}) \hat{\boldsymbol{k}}$ the component of $\boldsymbol{a}$ transverse to the photon momentum $\boldsymbol{k}$.

Evaluation of the operators $\mathscr{M}_i$ between the spinors (17) and (18) yields the following representation of the CGLN-amplitudes F_i in terms of the invariant amplitudes $\mathscr{A}_i$

$$F = G \mathscr{A} \tag{20}$$

with

$$G = f\, g\, a, \tag{21}$$

where f and a are diagonal matrices

$$f = \mathrm{diag}\,(1, \frac{kq}{E_f^+ E_i^+}, \frac{kq}{E_i^+}, E_f^-, \frac{E_\gamma}{E_i^+}, \frac{E_\gamma q}{k E_f^+}), \tag{22}$$

$$a = \mathrm{diag}\,(1, \frac{1}{k \cdot k}, 1, 1, \frac{1}{k \cdot k}, 1), \tag{23}$$

and

$$g = \frac{M_N N_i N_f}{4\pi i W} \begin{pmatrix} W^- & 0 & -k \cdot p_f & -k \cdot p_i & 0 & k \cdot k \\ -W^+ & 0 & -k \cdot p_f & -k \cdot p_i & 0 & k \cdot k \\ 0 & k \cdot k & W^+ & 0 & 0 & 0 \\ 0 & -k \cdot k & W^- & 0 & 0 & 0 \\ E_i^+ & o_1 & o_2 & -E_i^+ M_N & k^2 W & E_i^+ W^- \\ -E_i^- & -o_1 & o_3 & E_i^- M_N & -k^2 W & E_i^- W^+ \end{pmatrix}, \tag{24}$$

where we have introduced

$$E_i^{+/-} = E_i \pm M_N, \tag{25}$$

$$E_f^{+/-} = E_f \pm M_N, \tag{26}$$

$$W^\pm = W \pm M_N, \tag{27}$$

$$o_1 = E_\gamma k \cdot p_f - E_f k \cdot k, \tag{28}$$

$$o_2 = -p_f \cdot p_i - E_f M_N, \tag{29}$$

$$o_3 = k \cdot p_f - E_f W^-. \tag{30}$$

Inverting the matrix G yields the invariant amplitudes A_i expressed in terms of the CGLN-amplitudes F_i as follows

$$\mathscr{A} = G^{-1} F, \tag{31}$$

where

$$G^{-1} = \bar{h} \bar{f} \tag{32}$$

with

$$\bar{h} = \frac{2\pi i}{M_N W N_i N_f} \begin{pmatrix} E_i^- W & -E_i^+ W & 0 & 0 & 0 & 0 \\ 0 & 0 & k^2 W W^- & -k^2 W W^+ & 0 & 0 \\ 0 & 0 & k^2 W & k^2 W & 0 & 0 \\ -W^- & -W^+ & -c_{if} & -c_{if} & k \cdot k & k \cdot k \\ -k \cdot k & k \cdot k & -c_{if} W^- & c_{if} W^+ & k \cdot k W^- & -k \cdot k W^+ \\ -M_N & M_N & -d_{if} & -d_{if} & k \cdot p_i & k \cdot p_i \end{pmatrix}, \tag{33}$$

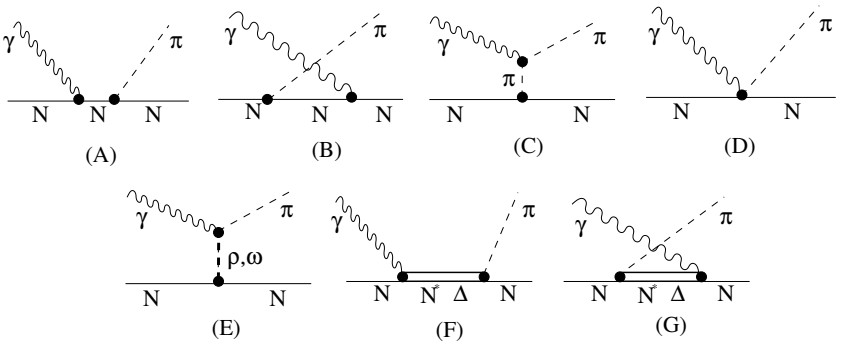

Fig. 1: Feynman diagrams for the $\gamma N \to \pi N$ amplitude. Born terms: (A) direct nucleon pole or s-channel, (B) crossed nucleon pole or u-channel, (C) pion in flight or t-channel, and (D) Kroll-Rudermann contact term; (E) vector-meson exchange; resonance excitations: (F) direct or s-channel and (G) crossed or u-channel.

introducing as a shorthand

$$c_{if} = \frac{1}{W}\left(k\cdot p_i k\cdot p_f - k\cdot k\, p_f\cdot p_i\right), \tag{34}$$

$$d_{if} = \frac{1}{W}\left(p_i\cdot p_i k\cdot p_f - k\cdot p_i\, p_f\cdot p_i\right), \tag{35}$$

and a diagonal matrix

$$\overline{f} = \mathrm{diag}\left(\frac{1}{E_i^-}, \frac{q}{kE_f^-}, \frac{1}{kqE_i^-}, \frac{1}{k^2E_f^-}, \frac{1}{E_\gamma E_i^-}, \frac{q}{E_\gamma kE_f^-}\right). \tag{36}$$

With the above mentioned relations, we can calculate scattering amplitudes for pion photoproduction on the nucleon in any frame of reference. The CGLN F_i amplitudes are given, although in the center of mass system. For the description of cross sections and polarization observables, we consider in the present work the Dubna-Mainz-Taipei dynamical model (DMT-2001) [28], the unitary isobar MAID model (MAID-2007) [29], and the chiral MAID model (χMAID-2013) [30].

The DMT-2001 model [28] is a unitary dynamical model based on a non-resonant background described by Born terms and vector-meson exchange contributions in the t-channel (ρ and ω) and the following 8 four-star nucleon resonances in the s-channel: $P_{33}(1232)$, $P_{11}(1440)$, $D_{13}(1520)$, $S_{11}(1535)$, $S_{31}(1620)$, $S_{11}(1650)$, $F_{15}(1680)$, and $D_{33}(1700)$. The DMT-2001 model describes the pion photo- and electroproduction observables in terms of photon and nucleon degrees of freedom and provides a very good description of experimental data in the near-threshold region. More information about the DMT-2001 model is given in Ref. [28] and we refer the reader to this reference for details.

The MAID-2007 model [29] is based on a non-resonant background described by Born terms (diagrams (A)-(D) in Fig. 1) and vector-meson exchange contributions in the t-channel (ρ and ω, diagram (E) in Fig. 1) and 13 four-star nucleon resonance excitations in the s-channel below 2 GeV (diagrams (F) and (G) in Fig. 1). The model uses effective Lagrangian methods to calculate the Born background, including ρ- and ω-meson exchange processes. The background amplitudes are unitarized with a $(1+if_{\ell\pm}^{\pi N})$ factor, where $f_{\ell\pm}^{\pi N}$ are the πN-scattering amplitudes. Moreover, the following four-star nucleon resonances were included in the MAID-2007 model: $P_{33}(1232)$, $P_{11}(1440)$, $D_{13}(1520)$, $S_{11}(1535)$, $S_{31}(1620)$, $S_{11}(1650)$, $D_{15}(1675)$, $F_{15}(1680)$, $D_{33}(1700)$, $P_{13}(1720)$, $F_{35}(1905)$, $P_{31}(1910)$, and $F_{37}(1950)$. These resonances are described by Breit-Wigner forms. The MAID-2007 model is parameterized in terms of invariant amplitudes and describes the pion photo- and electroproduction amplitudes in a consistent way. The isobar MAID-2007 model agrees with experimental observations very well (see Ref. [29] for detailed information).

The χMAID-2013 model [30] for studying pion photo- and electroproduction on the nucleon in the near-threshold region has been constructed in relativistic chiral perturbation theory and included all multipole amplitudes up to and including ℓ=4 or, in other words, G waves. This model provides a comprehensive description of the elementary process on the free nucleon up to photon energies of 170 MeV in the laboratory frame. Further information about the χMAID-2013 model is given in Ref. [30] and we refer the reader to this reference for details.

In the next section, we give numerical results for the unpolarized differential cross section $d\sigma/d\Omega_\pi$, the linear photon Σ-asymmetry, the the helicity E-asymmetry, and the double polarization F-asymmetry for the reaction channels $\gamma n \to \pi^0 n$, $\gamma p \to \pi^0 p$, $\gamma n \to \pi^- p$, and $\gamma p \to \pi^+ n$ in the photon energy region near threshold.

3 Results and discussion

Now, we will present and discuss our results for observables of $\gamma n \to \pi^0 n$, $\gamma p \to \pi^0 p$, $\gamma n \to \pi^- p$, and $\gamma p \to \pi^+ n$ reactions near threshold. In particular, we

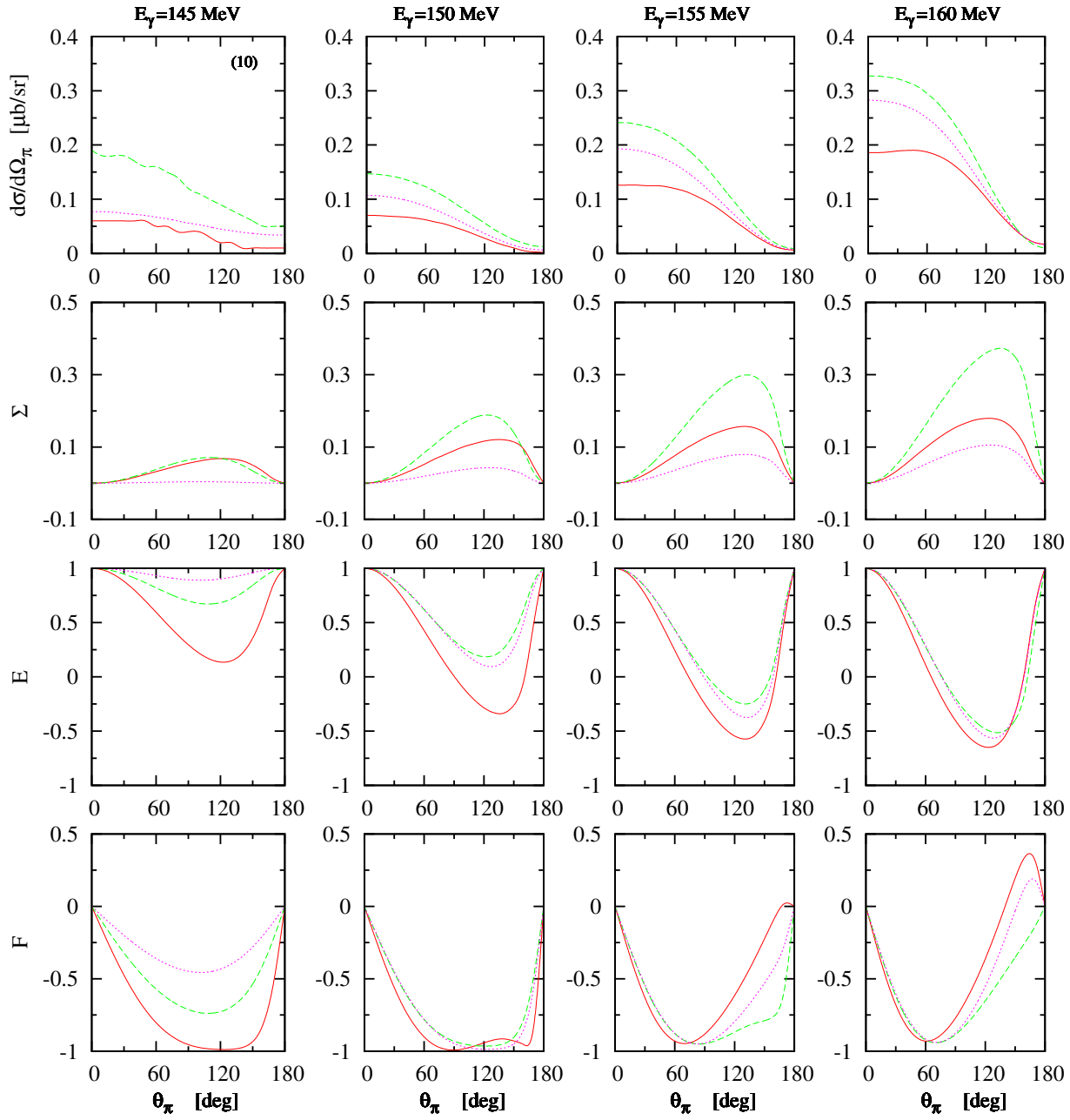

Fig. 2: (Color online) The unpolarized differential cross section $d\sigma/d\Omega_\pi$, linear photon Σ-asymmetry, E-asymmetry, and F-asymmetry for the reaction $\gamma n \to \pi^0 n$ as functions of pion angle in the c.m. frame at various photon lab-energies. The magenta-dotted, red-solid, and green-dashed curves represent the calculation using the DMT-2001 [28], MAID-2007 [29], and χMAID-2013 [30] models, respectively. Results for $d\sigma/d\Omega_\pi$ at E_γ=145 MeV are multiplied by the factor in the parentheses.

concentrate our discussion on results for the unpolarized differential cross section $d\sigma/d\Omega_\pi$, the linear photon Σ-asymmetry, the the helicity E-asymmetry, and the double polarization F-asymmetry. The pion photoproduction amplitude is evaluated in the present work by taking three different models which are the DMT-2001 [28], MAID-2007 [29], and χMAID-2013 [30].

We start the discussion with the results for observables of the $\gamma n \to \pi^0 n$ reaction ($E_\gamma^{\rm thr}$=144.67 MeV) as plotted in Fig. 2 as functions of pion angle in the c.m. frame at several fixed values of photon lab-energy

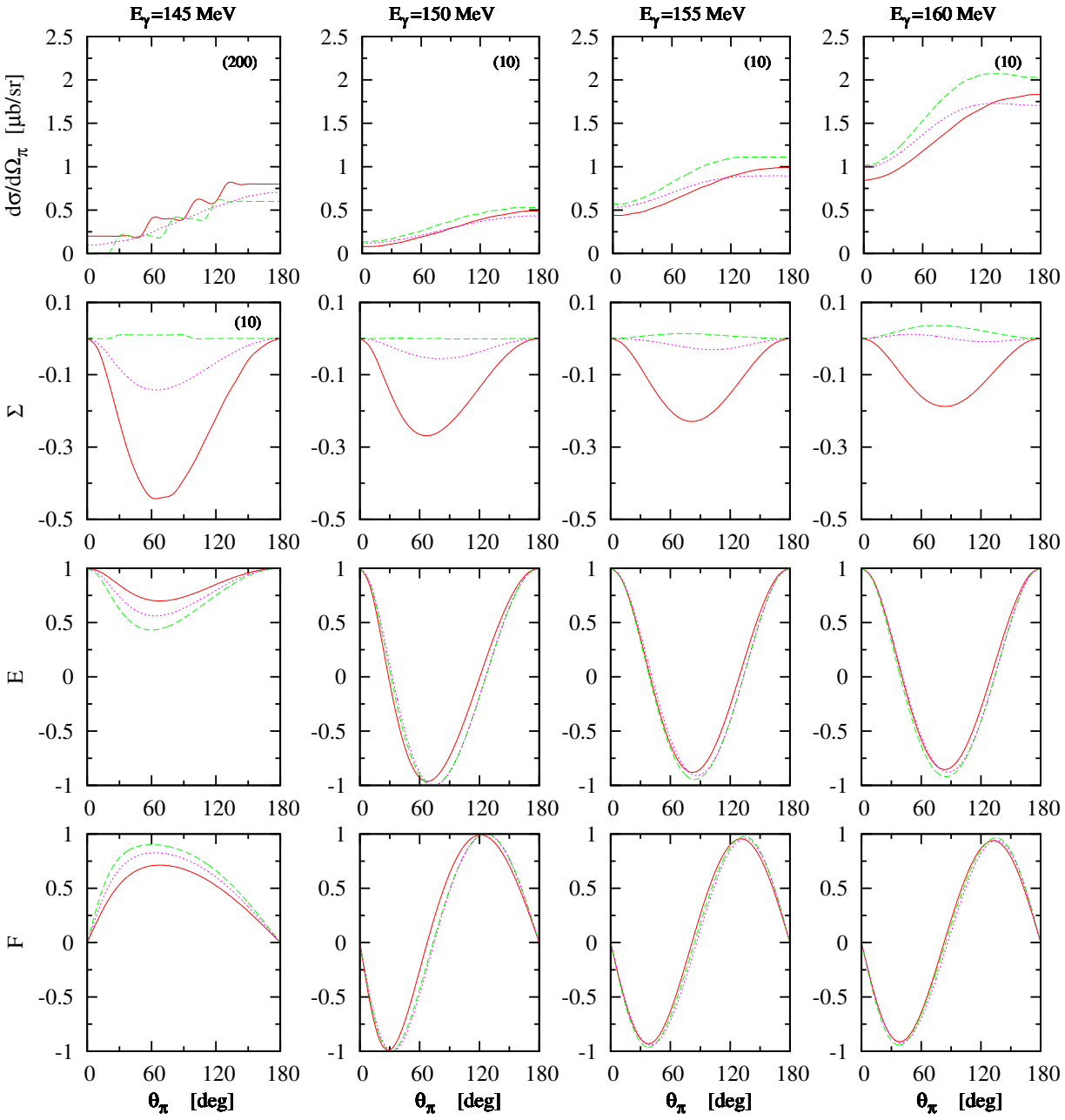

Fig. 3: (Color online) Same as in Fig. 2 but for the reaction $\gamma p \rightarrow \pi^0 p$. Results for $d\sigma/d\Omega_\pi$ are multiplied by the factor in the parentheses.

(E_γ=145, 150, 155, and 160 MeV). We see that the unpolarized differential cross section is strongly affected by the pion photoproduction amplitude, specially at forward pion angles. At pion angles greater than 120°, the differences between various models are small. As for the linear photon Σ-asymmetry, one can see that the big differences between the used models are seen in the peak position at about 120°. The same situation is seen in the case of the double polarization E-asymmetry with a longitudinal polarized nucleon target and a circularly polarized photon beam. In the latter case, one observes that the E-asymmetry is sensitive to the reaction amplitude at pion angle around 120° and at photon energies close to pion threshold. The dependence of the E-asymmetry on the reaction amplitude decreases with increasing the photon lab-energy. The same situation is seen in the case of the double polarization F-asymmetry. This means that the results for $\gamma n \rightarrow \pi^0 n$ observables are

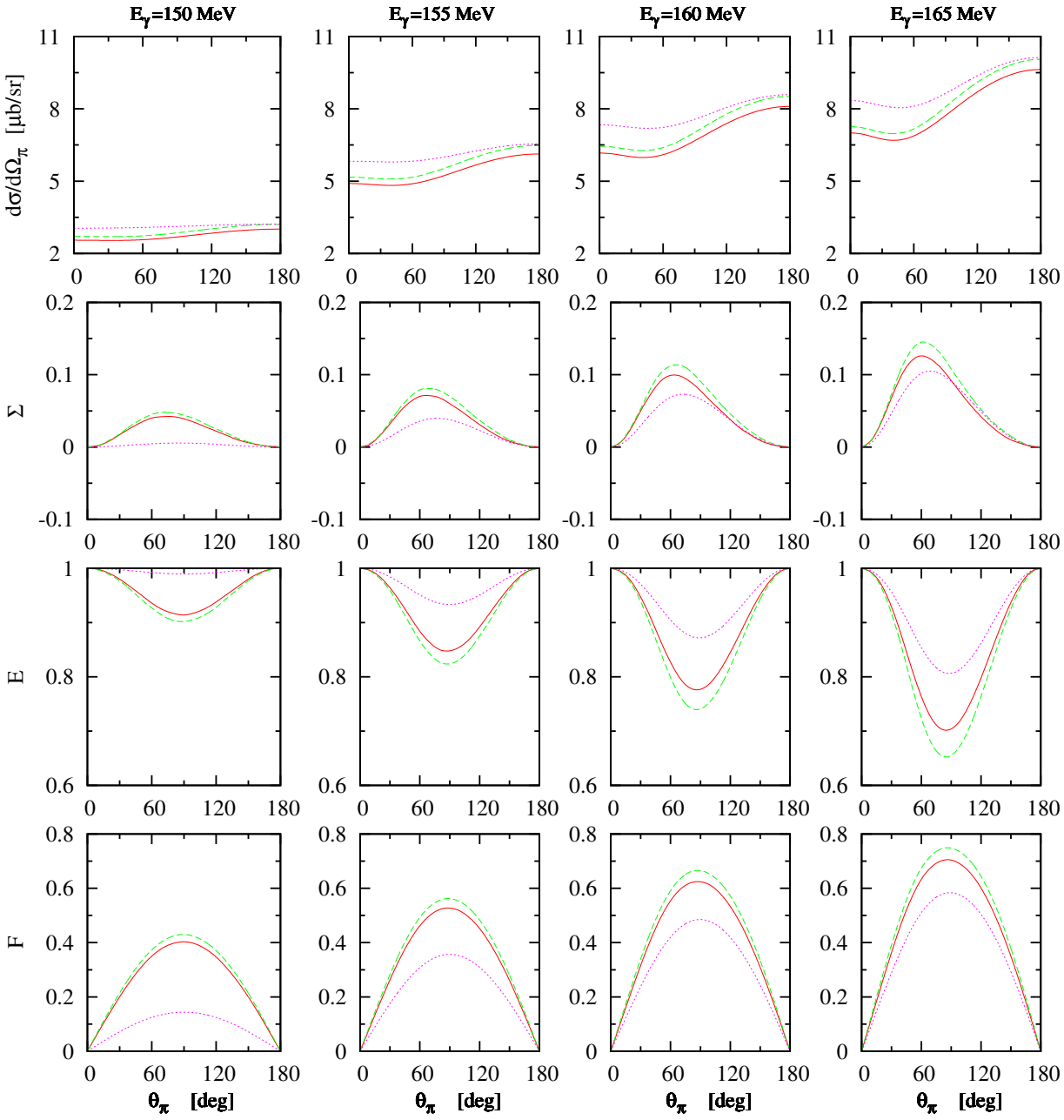

Fig. 4: (Color online) Same as in Fig. 2 but for the reaction $\gamma n \to \pi^- p$.

sensitive to the reaction amplitude since one obtains large differences between the results using various amplitudes.

As next, we discuss the results for the $\gamma p \to \pi^0 p$ ($E_\gamma^{\rm thr}$=144.68 MeV) as shown in Fig. 3 as functions of pion angle in the c.m. frame at several fixed values of photon lab-energy (E_γ=145, 150, 155, and 160 MeV). In contrast to the case of $\gamma n \to \pi^0 n$ reaction, we see here that the unpolarized differential cross section is not strongly affected by the pion photoproduction amplitude. The highest effect of reaction amplitude is seen at the highest photon energy. This is not the case for the Σ-asymmetry as one obtains big differences between the results for Σ using different reaction amplitudes in the peak position at about 65°. The sensitivity of E and F spin asymmetries to the reaction amplitude is very small is the case of $\gamma p \to \pi^0 p$ reaction. Only at the lowest photon energy, a small influence of E and F asymmetries on the reaction amplitude is obtained. This means that the results for $\gamma p \to \pi^0 p$ observables, instead of E-asymmetry, are insensitive to the reaction amplitude.

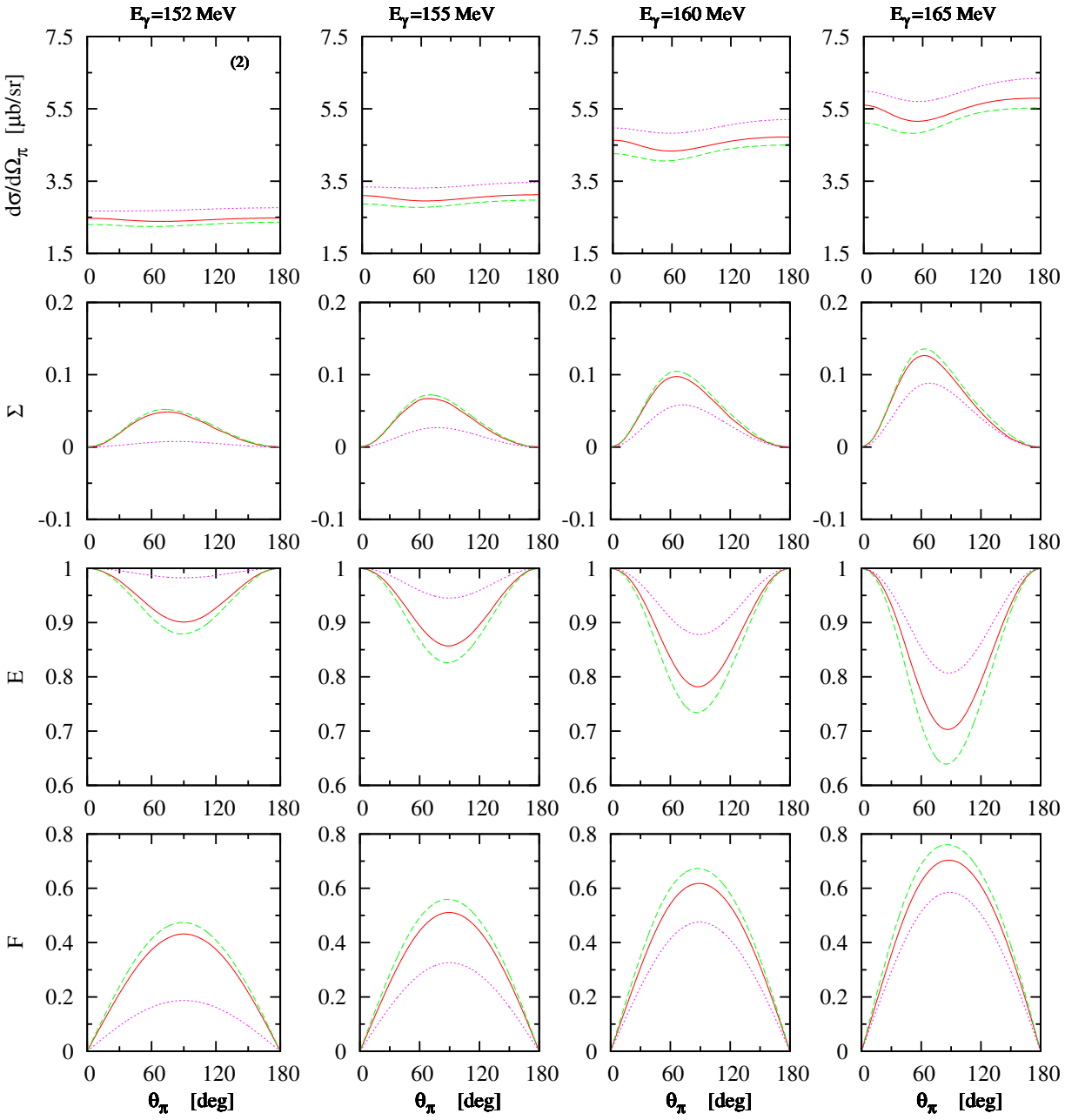

Fig. 5: (Color online) Same as in Fig. 2 but for the reaction $\gamma p \to \pi^+ n$. Results for $d\sigma/d\Omega_\pi$ at E_γ=152 MeV are multiplied by the factor in the parentheses.

Now, we start the discussion of the results for charged pion photoproduction channels $\gamma n \to \pi^- p$, and $\gamma p \to \pi^+ n$. At low photon energies, the charged pion reactions differ significantly in magnitude in comparison to the neutral channels due to the Kroll-Rudermann and pion pole terms which contribute only to the charged pion channels. In fact, in charged pion channels, where the electric dipole amplitude E_0^+ dominates at threshold, practically any calculation does not depend on the choice of the reaction amplitude. We would like to add that the Born terms play an important role in the case of charged pion production reactions at low photon energies.

The results for the $\gamma n \to \pi^- p$ observables ($E_\gamma^{\rm thr}$=148.46 MeV) are plotted in Fig. 4 as functions of pion angle in the c.m. frame at several fixed values of photon lab-energy (E_γ=150, 155, 160, and 165 MeV). In addition, the results for the $\gamma p \to \pi^+ n$ observables ($E_\gamma^{\rm thr}$=151.44 MeV) are shown in Fig. 5 as functions of

pion angle in the c.m. frame at E_γ=152, 155, 160, and 165 MeV. We see that the results for $\gamma n \to \pi^- p$ (Fig. 4) and $\gamma p \to \pi^+ n$ (Fig. 5) observables have qualitatively and quantatvely the same behavior. Furthermore, the big differences obtained in the results using various reaction amplitudes are approximately the same in both channels. We see also that the results for $\gamma n \to \pi^- p$ and $\gamma p \to \pi^+ n$ observables are sensitive to the reaction amplitude.

4 Conclusions

The main object of this work was to study the amplitude analysis of unpolarized differential cross section and polarization observables in the pion photoproduction reaction on the free nucleon in the photon energy region near threshold. Numerical results for the unpolarized differential cross section $d\sigma/d\Omega_\pi$, the linear photon Σ-asymmetry, the the helicity E-asymmetry, and the double polarization F-asymmetry for the reaction channels $\gamma n \to \pi^0 n$, $\gamma p \to \pi^0 p$, $\gamma n \to \pi^- p$, and $\gamma p \to \pi^+ n$ near threshold have been presented. We have investigated whether the uncertainties caused by the use of different $\gamma N \to \pi N$ amplitudes for the predictions of polarization observables in the $\gamma d \to \pi NN$ and $\gamma d \to \pi^0 d$ reactions are also seen in the analysis of observables for pion photoproduction on the nucleon. For this purpose, three different realistic models for the $\gamma N \to \pi N$ amplitude have been considered. These models are the unitary dynamical Dubna-Mainz-Taipei DMT-2001 model, the unitary isobar MAID-2007 model, and the chiral MAID (χMAID-2013) model. We found that the $\gamma n \to \pi^0 n$, $\gamma p \to \pi^0 p$, $\gamma n \to \pi^- p$, and $\gamma p \to \pi^+ n$ observables near threshold are sensitive to the production amplitude, specially at photon energies close to pion threshold.

In order to draw further conclusions, it would be very desirable to have precise experimental data for polarization observables in pion photoproduction on the nucleon near pion threshold. This clearly poses a more detailed test of the used models.

Conflicts of Interest

The authors declare that there is no conflict of interest regarding the publication of this article.

References

[1] A. Donnachie, *Photo- and Electroproduction Processes*, in *High Energy Physics* Vol. 5, edited by E.H.S. Burhop, Academic Press, New York, (1972).

[2] E.M. Darwish and H. Mansour, *Coherent π-production off deuteron near η-threshold: a theoretical overview*, LAP LAMBERT Academic Publishing, (2015).

[3] G.F. Chew, M.L. Goldberger, F.E. Low, and Y. Nambu, Phys. Rev. **106**, 1345 (1957).

[4] F.A. Berends, A. Donnachie, and D.L. Weaver, Nucl. Phys. B **4**, 1 (1967).

[5] F.A. Berends, A. Donnachie, and D.L. Weaver, Nucl. Phys. B **4**, 54 (1967).

[6] F.A. Berends, A. Donnachie, and D.L. Weaver, Nucl. Phys. B **4**, 103 (1967).

[7] R.D. Peccei, Phys. Rev. **181**, 1902 (1969).

[8] M.G. Olsson, Nucl. Phys. B **78**, 55 (1974).

[9] M.G. Olsson and E.T. Osypowski, Nucl. Phys. B **87**, 399 (1975).

[10] M.G. Olsson and E.T. Osypowski, Phys. Rev. D **17**, 174 (1978).

[11] R. Wittman, R. Davidson, and N.C. Mukhopadhyay, Phys. Lett. B **142**, 336 (1984).

[12] R. Davidson, N.C. Mukhopadhyay, and R. Wittman, Phys. Rev. Lett. **56**, 804 (1986).

[13] J.I. Sabutis, Phys. Rev. C **27**, 778 (1983).

[14] I. Blomqvist and J.M. Laget, Nucl. Phys. A **280**, 405 (1977).

[15] J.M. Laget, Phys. Rep. **69**, 1 (1981).

[16] H. Tanabe and K. Ohta, Phys. Rev. C **31**, 1876 (1985).

[17] S.-N. Yang, J. Phys. G **11**, L205 (1985).

[18] L. Heller, S. Kumano, J.C. Martinez, and E.J. Moniz, Phys. Rev. C **35**, 718 (1987).

[19] S. Kumano, Phys. Lett. B **214**, 132 (1988).

[20] G. Kaelbermann and J.M. Eisenberg, Phys. Rev. D **28**, 71 (1983).

[21] G. Kaelbermann and J.M. Eisenberg, Phys. Rev. D **29**, 517 (1984).

[22] M. Weyrauch, Phys. Rev. D **35**, 1574 (1987).

[23] S. Scherer, D. Drechsel, and L. Tiator, Phys. Lett. B **193**, 1 (1987).

[24] M. Araki and I.R. Afnan, Phys. Rev. C **36**, 250 (1987).

[25] R. Schmidt, H. Arenhövel, and P. Wilhelm, Z. Phys. A **355**, 421 (1996).

[26] H. Garcilazo and E.M. de Guerra, Phys. Rev. C **52**, 49 (1995); H. Garcilazo and E.M. de Guerra, Phys. Rev. C **49**, R601 (1994).

[27] F. Blaazer, B.L.G. Bakker, and H.J. Boersma, Nucl. Phys. A **568**, 681 (1994); F. Blaazer, B.L.G. Bakker, and H.J. Boersma, Nucl. Phys. A **590**, 750 (1995); F. Blaazer, PhD thesis, Free University of Amsterdam, (1995).

[28] S.S. Kamalov and S.N. Yang, Phys. Rev. Lett. **83**, 4494 (1999); S.S. Kamalov, S.N. Yang, D. Drechsel, O. Hanstein, and L. Tiator, Phys. Rev. C **64**, 03220(R) (2001); DMT-2001: https://maid.kph.uni-mainz.de/dmt/.

[29] D. Drechsel, S. Kamalov, and L. Tiator, Eur. Phys. J. A **34**, 69 (2007); MAID-2007: https://maid.kph.uni-mainz.de/maid2007/.

[30] M. Hilt, S. Sherer, and L. Tiator, Phys. Rev. C **87**, 045204 (2013); M. Hilt, B.C. Lehnhart, S. Sherer, and L. Tiator, Phys. Rev. C **88**, 055207 (2013); Chiral MAID: https://maid.kph.uni-mainz.de/chiralmaid/.

[31] W.J. Briscoe *et al.* [A2 Collaboration at MAMI], Phys. Rev. C **100**, 065205 (2019); W.J. Briscoe *et al.* [A2 Collaboration at MAMI], Eur. Phys. J. A **56**, 218 (2020).

[32] N.M. Kroll and M.A. Rudermann, Phys. Rev. **93**, 233 (1954).

[33] S. Fubini, G. Furlan, and C. Rossetti, IL Nuovo Cimento **40**, 1171 (1965).

[34] E.M. Darwish, C. Fernández-Ramírez, E. Moya de Guerra, and J.M. Udías, Phys. Rev. C **76**, 044005 (2007); M.I. Levchuk, Phys. Rev. C **82**, 044002 (2010); E.M. Darwish and S.S. Al-Thoyaib, Ann. Phys. (N.Y.) **326**, 604 (2011); E.M. Darwish *et al.*, Ann. Phys. (N.Y.) **411**, 167990 (2019); E.M. Darwish, M.M. Almarashi, and M. Saleh Yousef, Ann. Phys. (N.Y.) **420**, 168254 (2020); E.M. Darwish, M.I. Levchuk, M.N. Nevmerzhitsky, M.M. Almarashi, and M. Saleh Yousef, Chin. J. Phys. **71**, 319 (2021).
[35] E.M. Darwish and H. Al-Ghamdi, Moscow Uni. Phys. Bull. (2021), in press.
[36] J.D. Bjorken and S.D. Drell, *Relativistic Quantum Mechanics*, McGraw-Hill, New York, (1964).
[37] J. Lippmann and W. Schwinger, Phys. Rev. **84**, 1232 (1951).
[38] E.M. Darwish and S.S. Al-Thoyaib, Arab. J. Sci. Eng. **33**, 401 (2008).